Macroscopic Evidence of Enhanced Formation of Methane Nanohydrates in Hydrophobic Nanospaces

J. Miyawaki,[†] T. Kanda,[†] T. Suzuki,[†] T. Okui,[‡] Y. Maeda,[‡] and K. Kaneko*[,†]

Physical Chemistry, Material Science, Graduate School of Science and Technology, Chiba University, 1-33 Yayoi, Inage, Chiba 263, Japan, and Frontier Technology Research Institute, Tokyo Gas Co., 1-7-7 Suehiro, Tsurumi, Yokohama, 230, Japan

Received: October 31, 1997; In Final Form: January 16, 1998

The methane adsorption of water-preadsorbed carbons of different micropore widths w at 303 K was measured. Although the amount of adsorption of supercritical methane on microporous carbon at 303 K was less than 9.4 mg g^{-1} at 101 kPa, the presence of the preadsorbed water enhanced noticeably the methane adsorption at 303 K even under subatmospheric pressure. The adsorption increment of methane reached a maximum at 1−2 h after introduction of methane and decreased gradually to a steady value after 20−50 h. The adsorption increment of methane depended on the fractional filling ϕ_w of micropores by the preadsorbed water. The maximum increment of 110 mg g^{-1} for $w = 1.1$ nm at a methane pressure of 2.6 kPa was obtained at $\phi_w = 0.34$, corresponding to the estimated adsorption amount at 21 MPa of methane (130 mg g^{-1}). The methane-adsorption increment increased linearly with ϕ_w until $\phi_w = 0.35$, indicating the formation of the stable methane−water clathrate of which the composition of methane to water is 1:2. Thus, the nano-order hydrates of methane should be formed in the micropore. The plausible model of the nanohydrate was proposed on the basis of the experimental results and simulation of methane adsorption.

Introduction

Clathrate compounds had been actively studied 30−40 years ago. Molecules having hydrogen-bonding ability can produce hydrogen-bonded network structures with voids, which can occlude guest molecules. Molecular hydrate is the representative of molecular clathrates. In particular, recently methane hydrate has gathered much attention because of its environmental importance and new energy resources. The huge amounts of methane hydrates are widely found in the ocean bed and permafrost regions. Hence, methane hydrate is an essentially important substance in earth science. The hydrate structures are composed of the polyhedral formed by hydrogen-bonded water molecules. There are two solid types of methane hydrates of structure I. The structure I has two kinds of cavities of which radii are 0.391 and 0.433 nm. It is well-known that the ideal water/methane ratio of structure I of 5.75 can occupy both cavities of structure I. The crystal system and lattice structure of structure I are cubic and body-centered, respectively, and the lattice constant is 1.2 nm.[1,2]

The stable methane hydrate formation needs more than 80 MPa at 303 K.[3] The formation mechanism is not sufficiently elucidated. The important role of pores in minerals in the formation of the methane hydrates in the ocean bed has been pointed out. Handa examined the thermodynamic formation conditions of methane hydrates in mesopores of silica gel (pore width =14 nm).[4] Cha et al. reported that the presence of montmorillonite increases the hydrate-stability temperature and suggested the importance of adsorbed water.[5] Macropores or mesopores can contribute to the stabilization of methane hydrates without steric hindrance. To produce methane hydrates having crystal structures that are the same as structure I, the pore width should be greater than the sum of the lattice constant and the oxygen diameter at least.

Molecules are adsorbed on the macropore surface with a layer-by-layer mechanism, on mesopores by capillary condensation, and in micropores by micropore filling. Recent fundamental research on micropore filling elucidated the presence of a strong molecule−surface interaction overlapped from opposite pore walls. The substantial adsorption begins at an extremely low pressure. The active molecular-simulation studies showed the successive steps of adsorption,[6−8] that is, monolayer adsorption on the pore walls and filling in the residual space between the monolayer-coated pore walls. Activated carbon is composed of nanographites, which provide the micropore walls. The almost-parallel configuration of the nanographites gives the slit-shaped micropores. In particular, the recently developed activated carbon fiber (ACF) and superhigh surface-area carbon (SAC) have very uniform micropores of the great pore volume, compared with the conventional activated carbon. The recent studies on molecular assemblies confined in the micropore showed organized molecular structures.[9] Kaneko et al. found that NO molecules are dimerized, inducing the high-pressure disproportionation reaction of the NO dimer in the micropore without application of high pressure.[10,11] Hence, molecules confined in micropores behave as if they were exposed to a high pressure. Iiyama et al. showed that water molecules confined in the carbon micropores form an ordered structure-like solid even at 303 K by in situ X-ray diffraction.[12,13] Also, it was reported that the ordered adsorbed water forms a kind of clathrate compound with NO in the carbon micropore.[14] Water molecules do not adsorb in carbon mesopores of hydrophobicity. The predominant intermolecular interaction of a water molecule is not the dispersion interaction but the electrostatic interaction, which induces the hydrogen bonding.

* To whom correspondence should be addressed. Fax: 81-43-290-2788. E-mail: kaneko@pchem1.nd.chiba-u.ac.jp.
[†] Chiba University.
[‡] Frontier Technology Research Institute.

S1089-5647(98)00034-0 CCC: $15.00
Published on Web 02/26/1998

A water molecule does not strongly interact with the graphitic surface compared with the intermolecular interaction. Hence, the adsorption isotherm of water on activated carbon is of type V. Müller et al. studied water adsorption in the graphite slit pore and examined the effect of the polar sites on the water adsorption using GCMC simulation, suggesting the formation of a two-dimensional hydrogen-network structure.[15] This result coincides with the above-mentioned X-ray diffraction study. Therefore, it is expected that adsorbed water molecules of a two-dimensional network structure form a new molecular compound with a methane molecule in the hydrophobic micropore. This paper describes a noticeable enhancement of methane adsorption by the preadsorbed water in carbon micropores.

Experimental and Simulation

Microporous Carbon Samples and Their Characterization. We used four kinds of steam-activated pitch-based ACFs (P5, P10, P15, and P20) and the KOH-activated pitch-based SAC (SAC31). The micropore structures were determined by the high-resolution nitrogen adsorption isotherm at 77 K using a computer-aided gravimetric apparatus. The micropore structures were determined from a high-resolution α_s-plot analysis for the nitrogen isotherm. The X-ray diffraction of ground carbon samples was measured by use of Cu Kα radiation with an automatic diffractometer.

Mixed-Gas Adsorption. The adsorption isotherms of water vapor on samples were measured gravimetrically. The pure-methane adsorption isotherms were measured at 303 K up to 10 MPa using the gravimetric equipment. The mixed-gas adsorption isotherms of methane and water on samples were measured at 303 K with the gravimetric method in two ways. One is the premixed-gas method in which water and methane gases mixed in advance are adsorbed on carbon at 303 K. Another is the preadsorbed-water method in which methane was adsorbed on the carbon having preadsorbed water in the micropore. Since methane is a supercritical gas at 303 K, only a small amount of methane is adsorbed on carbon without application of high pressure above 101.32 kPa. We measured the water-vapor content in the gas phase before and after introduction of methane with the Karl−Fisher method; the gas-phase content was kept constant within ±5%. Therefore, the enhancement in methane adsorption indicates the presence of the strong interaction between water and methane molecules such as the methane hydrate formation.

Grand Canonical Monte Carlo (GCMC) Simulation of Methane Adsorption. The possible adsorbed structure of pure methane in the graphite-slit pore was examined by the GCMC simulation. We used the one-center approximation for the methane molecule. The 12-6 Lennard-Jones potential (eq 1) $\Phi(r)$ for the interaction between a methane molecule (f) and a carbon atom (s) as a function of the distance r between them were used:

$$\Phi(r) = 4\epsilon_{sf}[(\sigma_{sf}/r)^{12} - (\sigma_{sf}/r)^{6}] \quad (1)$$

where ϵ_{sf} and σ_{sf} are the potential-well depth and effective diameter for the admolecule−graphitic carbon atom, respectively. These cross parameters are calculated according to the Lorentz−Berthelot rules, $\epsilon_{sf} = (\epsilon_{ss}\epsilon_{ff})^{1/2}$; $\sigma_{sf} = (\sigma_{ss} + \sigma_{ff})/2$. Here, ($\sigma_{ss}$, ϵ_{ss}) and (σ_{ff}, ϵ_{ff}) are the Lennard-Jones parameters for a surface atom and a molecule, respectively. The used parameters were $\sigma_{ss} = 0.340$ nm, $\epsilon_{ss}/k_B = 28.3$ K, $\sigma_{ff} = 0.381$ nm, and $\epsilon_{ff}/k_B = 148.1$ K. The interaction potential $\Phi(z)$ for an admolecule and a single graphite slab is given by the Steele 10-4-3 potential:[16]

$$\Phi(z) = 2\pi\rho_C\epsilon_{sf}\sigma_{sf}^{2}\Delta\{(2/5)(\sigma_{sf}/z)^{10} - (\sigma_{sf}/z)^{4} - \sigma_{sf}^{4}/[3\Delta(0.61\Delta + z)^{3}]\} \quad (2)$$

where z is the vertical distance of the admolecule above the surface, Δ is the separation between graphite layers, and ρ_C is the number density of carbon atoms in a graphite layer. Both Δ and ρ_C were determined from the X-ray diffraction. The interaction potential $\Phi_p(z)$ of the molecule confined in the slit pore is given by

$$\Phi_p(z) = \Phi(z) + \Phi(H - z) \quad (3)$$

Here, H is the physical width. The 12-6 Lennard-Jones potential was also used for the methane−methane interaction. We used the established technique of the GCMC simulation.[17] For comparison with the experimental result, we adopted the simplest approximation for the relationship between the physical width H and the experimental pore width w:

$$w = H - \sigma_{ss} \quad (4)$$

The GCMC simulation was performed for the graphitic-slit system of $w = 1.2$ nm. The size of the unit cell was 6×6 nm^2. The GCMC simulation was basically run for 2×10^6 configurations to get an equilibrium using the Hewlett-Parkard 735 workstation.

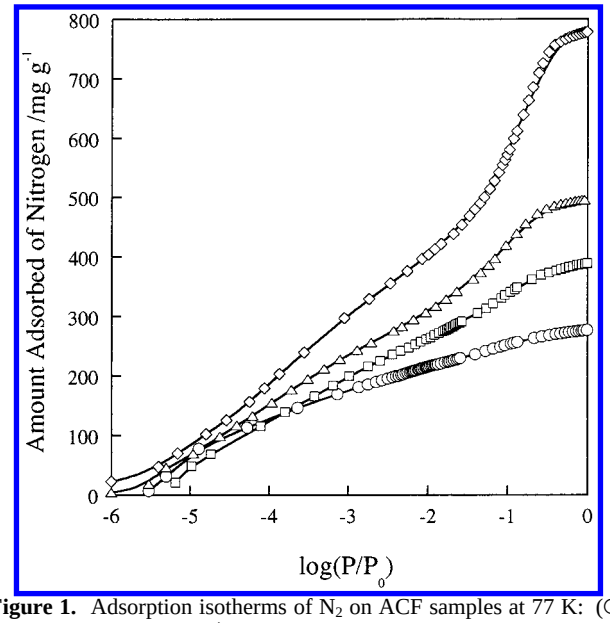

Figure 1. Adsorption isotherms of N_2 on ACF samples at 77 K: (○) P5; (□) P10; (△) P15; (◇) P20.

Results and Discussion

Pore Structures of Carbon Samples. N_2 adsorption isotherms of all ACFs and SAC (SAC31) were basically of type I, although N_2 adsorption isotherms of P20 and SAC31 had a linear increase until $P/P_0 = 0.4$ after a marked uptake in the low-pressure region. Since the adsorption data in the extremely low relative-pressure region are quite important in case of the micropore characterization, the N_2 adsorption isotherms of which the abscissa is expressed by the logarithm of P/P_0 are shown in Figure 1. The uptake below $\log(P/P_0) = -3$, where monolayer adsorption starts on each pore wall, gradually increases with P/P_0. P20 has a steep uptake near $\log(P/P_0) = -1$. The N_2

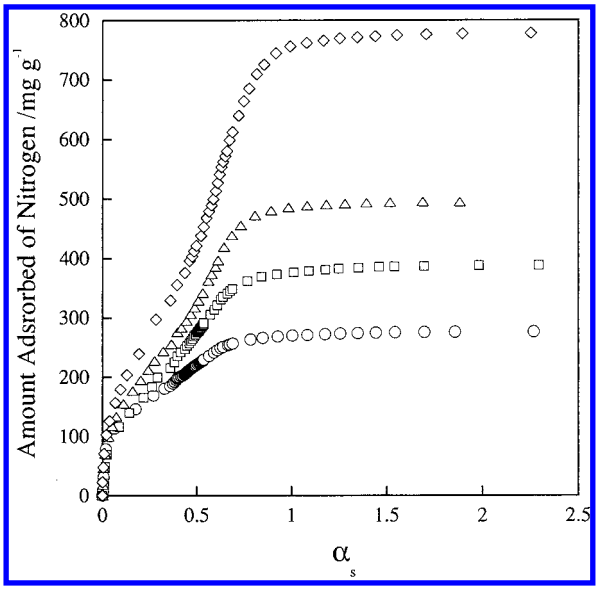

Figure 2. High-resolution α_s plots for the N_2 adsorption isotherms of ACF samples: (○) P5; (□) P10; (△) P15; (◇) P20.

TABLE 1: Micropore Structural Parameters

	specific surface area $m^2\ g^{-1}$	pore volume $cm^3\ g^{-1}$	average pore width nm
P5	900	0.336	0.75
P10	960	0.407	0.86
P15	1310	0.599	0.94
P20	1800	0.946	1.1
SAC31	2290	1.33	1.2

adsorption isotherms were analyzed by the high-resolution α_s plot. Figure 2 shows the high-resolution α_s plots. The α_s plot of P5 has a marked filling swing, indicating the presence of uniform micropores of less than 0.75 nm. On the other hand, the α_s plot of P20 has both of the filling and cooperative swings, indicating the presence of larger micropores. The α_s plots of other samples have both swings due to the presence of pores of medium pore width. We determined the micropore volume, the surface area, and the average pore width with the aid of subtracting the pore-effect method using the high-resolution α_s plot.[18,19] The theoretical background of the SPE method was recently given by authors using the GCMC simulation.[19] Table 1 collects the micropore structural parameters. The micropore width of these samples is in the range 0.75−1.2 nm.

Water Adsorption Isotherms. Figure 3 shows the water adsorption isotherms of P5, P10, and P20 at 303 K. All adsorption isotherms are of type V. The adsorption uptake at the low P/P_0 region is nil, indicating that surface functional groups are few and that the micropore walls are hydrophobic. The adsorption isotherms of P10 and P20 have a steep rise at $P/P_0 = 0.5$ and 0.7 with a marked hysteresis, respectively, while the isotherm of P5 rises near $P/P_0 = 0.4$ and has a slight hysteresis. The water adsorption isotherm of SAP31 was similar to that of P20. In the previous study,[20,21] we associated the difference of the adsorption hysteresis with cluster formation and the cluster size of water molecules. The saturated amount of water adsorption is briefly close to the micropore volume from N_2 adsorption. Then water molecules are adsorbed in micropores in the form of clusters at the beginning of adsorption. At medium relative pressure, those clusters merge to form a solidlike structure according to the preceding in situ X-ray-diffraction study.[12]

Enhanced Methane Adsorption by Preadsorbed Water. The adsorption amount of methane and water mixed in advance

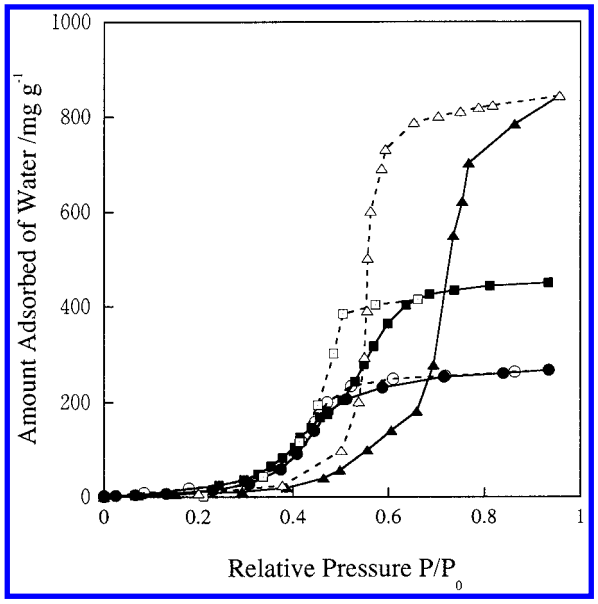

Figure 3. Adsorption and desorption isotherms of water on ACF samples at 303 K. The solid and open symbols denote adsorption (Ads.) and desorption (Des.) isotherms, respectively: (●) P5 Ads.; (○) P5 Des.; (■) P10 Ads.; (□) P10 Des.; (▲) P20 Ads.; (△) P20 Des.

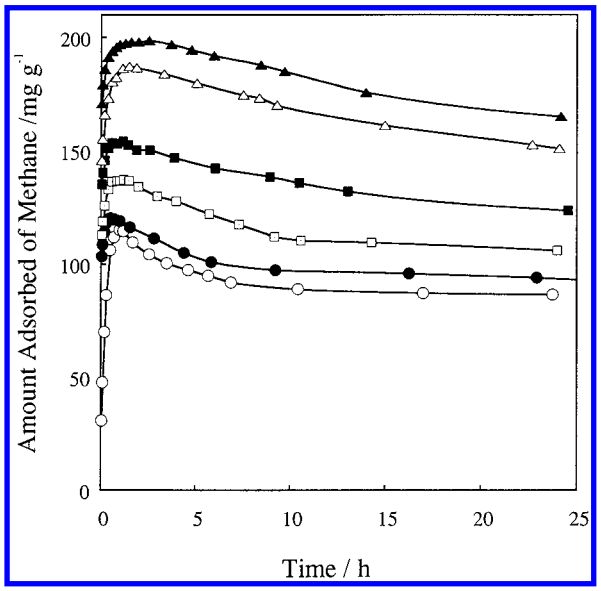

Figure 4. Time dependence of methane adsorption on water-preadsorbed P20 ($\phi_w = 0.28$) at 303 K at (○) 1.52, (●) 2.99, (□) 5.55, (■) 10.5, (△) 18.6, and (▲) 32.0 kPa.

(CH_4/H_2O [=2.49 kPa] ratio of 1.0 and 4.8) was almost the same as the adsorption isotherm of pure water because the methane adsorption at 303 K is almost negligibly small at the subatmospheric pressure of methane (<9.4 mg g^{-1} at 101 kPa). In contrast, the preadsorbed-water method showed an unusual adsorption behavior. The volume fractional filling ϕ_w of the pore volume by the preadsorbed water varied in the range 0.08−0.64. The adsorption rate of methane on water-preadsorbed P20 of the volume fractional filling $\phi_w = 0.28$ at 303 K upon introducing methane of different pressures for 25 h is shown in Figure 4. The adsorption proceeds rapidly and noticeably in the presence of the preadsorbed water. The adsorption increment reaches a maximum at 1−2 h after introduction of methane and decreases gradually to become a steady value after 10−25 h. The time dependences of the adsorption increment at different methane pressures are almost similar to each other.

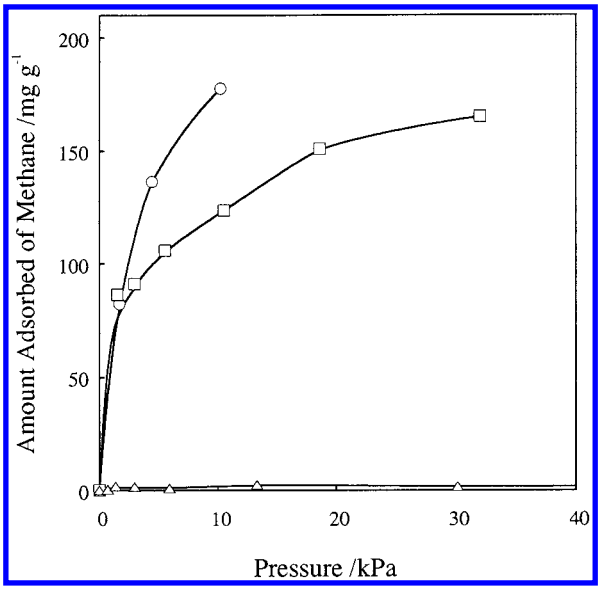

Figure 5. Adsorption isotherms of methane on P20 having different amounts of preadsorbed water at 303 K: (○) $\phi_w = 0.40$; (□) $\phi_w = 0.28$; (△) $\phi_w = 0$.

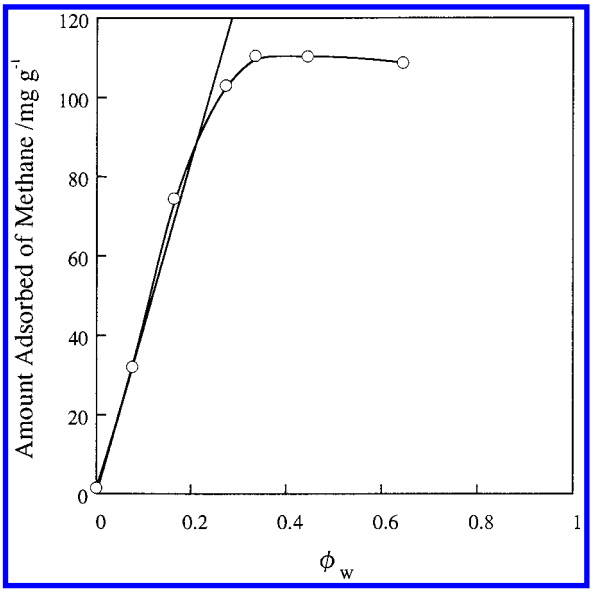

Figure 6. Relationship between the volume fractional filling by preadsorbed water and the amount of methane adsorption of P20 at 303 K at a methane pressure of 2.6 ± 0.1 kPa.

This adsorption uptake is caused by the adsorption of only methane because of the above-mentioned gas analysis. Hence, the adsorption increment upon introducing methane is expressed as the amount of adsorbed methane in Figure 4. Since very small amounts of gases were introduced for 10 min in order to avoid the Joule−Thomson effect, we presumed no temperature drop and the initial adsorption increment is not caused by water adsorption but by excess adsorption of methane near the pore. Since the uniform stable structure of preadsorbed water and methane is formed in the pore and then the pressure approaches an equilibrium value, the adsorbed excess methane should be desorbed. Therefore, the gradual decrease of methane adsorption should be attributed to conversion of a transient structure to a stable one. Figure 5 shows adsorption isotherms of methane on the water-preadsorbed P20 at 303 K as a function of ϕ_w. Here, we used the steady values after 24 h as the amount of methane adsorption. The amount of adsorbed methane is almost nil in the absence of the preadsorbed water, as mentioned above. In contrast, abundant methane of more than 100 mg g^{-1} is adsorbed on the water-preadsorbed P20 even below 10 kPa for $\phi_w = 0.28$. In the case of $\phi_w = 0.40$, the adsorption of methane at 10 kPa is greater than 180 mg g^{-1}. When water is not preadsorbed, the amount of adsorption for methane of 10 MPa on the same ACF is only 125 mg g^{-1} according to the high-pressure adsorption experiment. Thus, the presence of preadsorbed water gives rise to a remarkable enhancement of methane adsorption.

The enhanced methane adsorption strongly depended on the amount of the preadsorbed water in micropores. Figure 6 shows the relationship between the amount of the enhanced methane adsorption and ϕ_w at a methane pressure of 2.6 kPa. The enhanced methane adsorption increases linearly up to $\phi_w = 0.3$, accompanying a slight decrease with ϕ_w. This linear rise passes the origin, indicating the formation of a stable compound between methane and water molecules in the carbon micropore. The slope of the linear relation corresponds to the composition of methane/water = 1:2 in the molar ratio for the stable molecular compound. We call this compound methane nanohydrate. As mentioned later, the structure of this methane nanohydrate is considered as a stacked structure of two-dimensional sheets of water and of methane. Hence, it may be

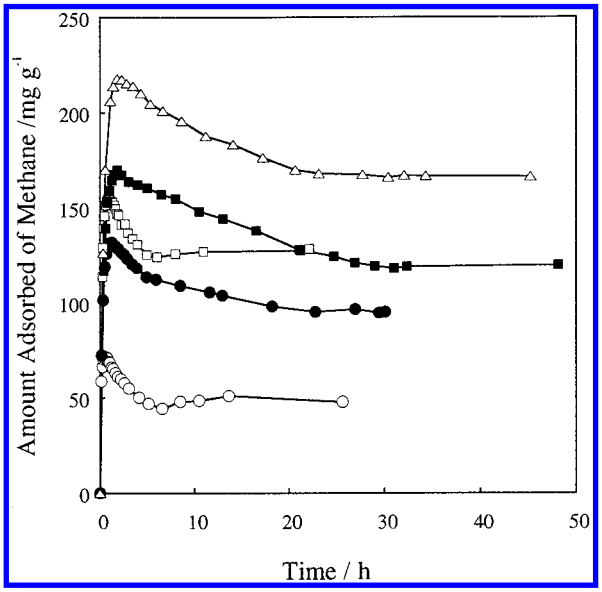

Figure 7. Temperature dependence of methane adsorption rate on water-preadsorbed P20 ($\phi_w = 0.3$) at 303 K: (○) 293 K; (●) 298 K; (□) 303 K; (■) 308K; (△) 313 K.

called a new type of molecular clathrate compound. The composition of the methane nanohydrate is different from that of the bulk methane hydrate (methane/water = 1:5.75).[1] The lattice constant of the bulk methane hydrate crystal of type I is 1.2 nm, being greater than the pore width of the used carbons. Since the micropore walls can play the role of host for methane molecules, the water content of methane nanohydrate is smaller than that of the bulk methane hydrate. Thus, the methane nanohydrate formed in the carbon micropore should have a structure different from that of the bulk hydrate crystal.

Temperature and Pore-Width Dependence of Enhanced Methane Adsorption. The adsorption rates of methane on the water-preadsorbed P20 ($\phi_w = 0.3$) at different temperatures upon introducing methane of different pressures for 25 h are shown in Figure 7. The adsorption rate at 308 K is almost similar to that at 303 K, while the methane uptake at 298 K is considerably small compared with that at 303 K. The higher the temperature, the greater the equilibrium methane adsorption. Although the

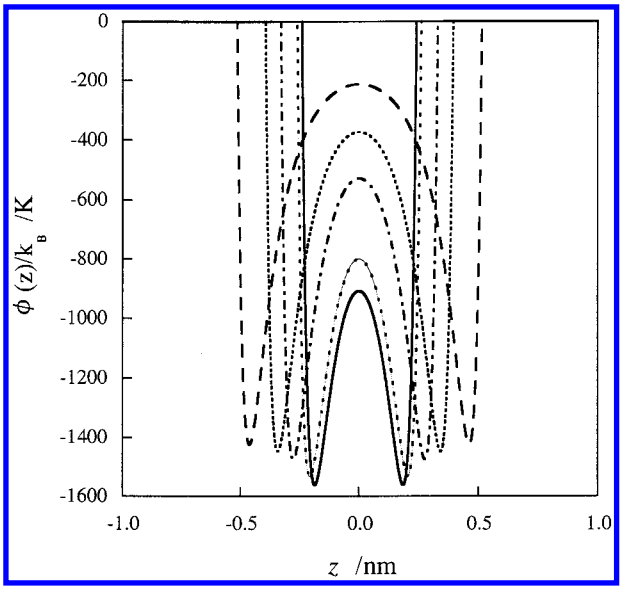

Figure 8. Interaction profiles of a methane molecule with the graphite-slit pore for different pore widths: (−) $w = 0.75$ nm; (- - -) $w = 0.79$ nm; (-·-) $w = 0.94$ nm; (···) $w = 1.1$ nm; (− − −) $w = 1.3$ nm.

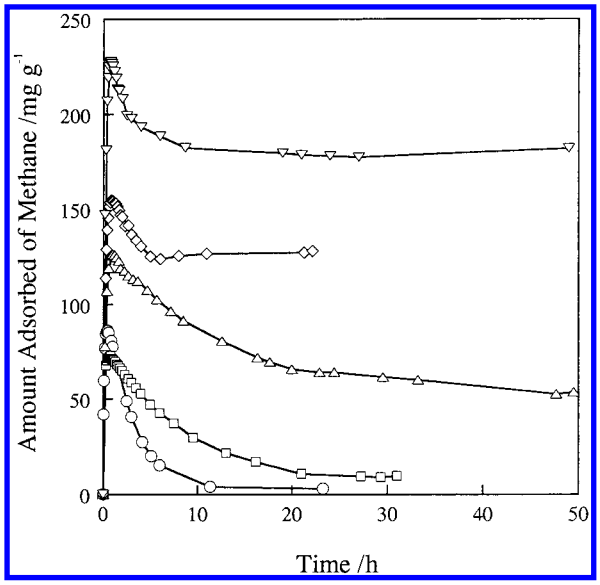

Figure 9. Methane adsorption rates on water-preadsorbed carbon samples at 303 K: (○) P5; (□) P10; (△) P15; (◇) P20; (▽) SAC31.

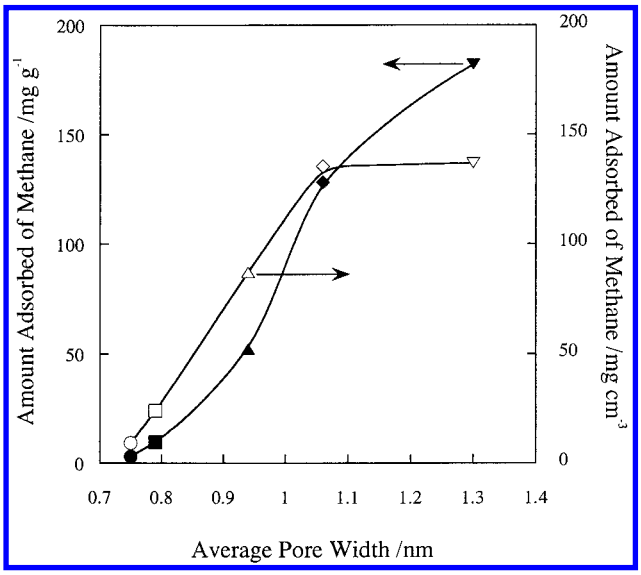

Figure 10. Relationships between the amount adsorbed of methane and average pore width at 303 K. The solid and open symbols denote the amounts adsorbed or methane per gram adsorbent and per unit pore volume, respectively: (○, ●) P5; (□, ■) P10; (△, ▲) P15; (◇, ◆) P20; (▽, ▼) SAC31.

lower temperature is favorable for the bulk methane hydrate, the above result has the opposite tendency. Since the diffusion of methane molecules is indispensable to form the clathrate compound in a highly restricted nanospace, the kinetic factor should be predominant. This temperature dependence suggests the importance of the mobility of adsorbed water molecules in the formation of the methane nanohydrate.

The interaction potential of a methane molecule with the graphitic slit is essential for producing the methane nanohydrate in micropores. Figure 8 shows the interaction potential profiles of a methane molecule with the graphite slit for different pore widths in the absence of water molecules. Here, the coordinate is transferred into the vertical distance z from the midplane of the pore. All potential profiles have a double minimum, and thereby, supercritical methane molecules tend to be adsorbed on the double-minima positions at first under the high-pressure conditions at 303 K; that is, methane molecules form the monolayer on the slit pore walls at a sufficiently high pressures of methane at 303 K. The smaller the pore width, the deeper the potential depth. The difference in the potential depth among these pores is 200 K, which can affect the enhancement of methane adsorption at 303 K. The effect of the pore width on the stability of the methane−water clathrate should be examined. Figure 9 shows the adsorption rate of methane on various carbon samples of different pore widths. P15, P20, and SAC31 have a remarkable enhancement of methane adsorption. The absolute amount of enhancement varies with the pore volume of the samples. However, P5 and P10 show the clear uptake at 1 h after introduction of methane, but the uptake decreases with time. The steady value of methane adsorption on P5 after 23 h is only 3.1 mg g^{-1}. Figure 10 shows the relationships between methane adsorption and pore width at 303 K. Here, the left- and right-side ordinates denote methane adsorption per gram of adsorbent and that per unit pore volume, respectively. The methane adsorption per gram of adsorbent increases with the pore width owing to the increase of the pore volume, whereas the methane adsorption per unit pore volume steeply increases with the pore width and reaches a plateau over 1 nm. This relation indicates the presence of the best size for nanohydrate formation. Although a smaller pore has a stronger interaction potential with a methane molecule, there is a restriction of nanohydrate formation. Hence, the pore width of 1.05 nm at least is necessary for abundant formation of methane nanohydrate. The structural model should satisfy these geometrical conditions and the stable composition of the methane nanohydrate.

Possible Nanoclathrate Structure of Water and Methane. The GCMC simulation gives a good description of methane molecular structure in the graphitic-slit pore in the absence of preadsorbed water.[22] We can approximate the adsorbed molecular state in the water-preadsorbed micropores by that under a high pressure of methane without the preadsorbed water because a water molecule is repelled by the graphitic-pore walls, whereas methane molecules are attracted by the dispersion force, as mentioned before. However, when water molecules form a cluster, the weak dispersion interaction should work for the water cluster and graphitic-pore system, being adsorbed above the medium relative pressure. Figure 11 shows a snapshot of methane molecules in the micropore from the GCMC simulation

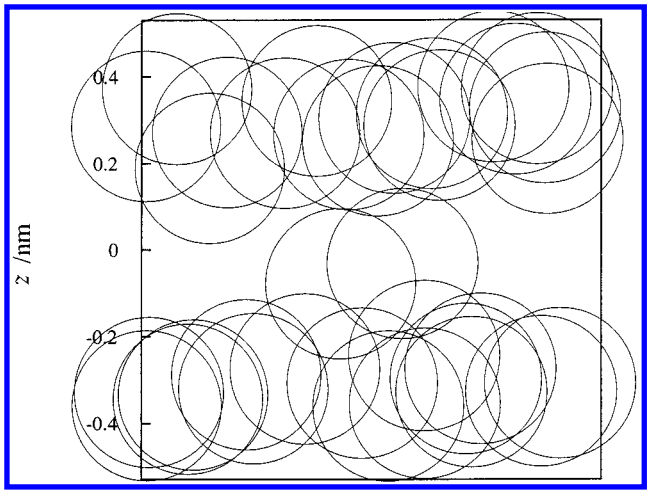

Figure 11. Snapshot of adsorbed methane molecules in the micropore $w = 1.1$ nm at a methane pressure of 14 MPa and 303 K.

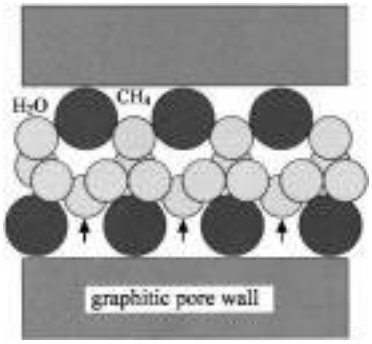

Figure 12. Possible model of methane nanohydrate in the pore. Larger and smaller spheres denote methane and water molecules, respectively. The arrow denotes a water connecting two water clusters.

without the preadsorbed water for a pore width of 1.1 nm. The amount adsorbed of methane on P20 ($w = 1.1$ nm) in Figure 5 just corresponds to the monolayer adsorption of the simulated isotherm. Accordingly, we presume that methane molecules are adsorbed on the pore wall in the presence of water at subatmospheric pressures of methane. The preadsorbed water should play a role of application of high pressures. The water molecules repelled from the graphitic-pore walls are associated with each other to form the hydrogen-bonded zigzag chain at the central space of the micropore. The zigzag structure can interact with a methane molecule through the dipole−octapole interaction. At the same time, adsorbed water molecules themselves are stabilized by the coexistence of the monolayered methane molecules. Figure 12 shows the model structure of the methane nanohydrate in the micropore of $w = 1.1$ nm. The methane molecules occupy the double-potential minima of the overlapped molecule−graphitic-pore wall interaction; they form the monolayer on the micropore walls. The micropores of ACF of 1.1 nm in width can accept the bilayer adsorption of methane molecules in the positions of the double-potential minima, if a high pressure of methane is applied. On the other hand, water molecules avoid the hydrophobic graphitic-pore walls and thereby they are associated with each other to produce the zigzag chain of clusters at a central vacancy between the array structures of methane molecules. This zigzag chain of water clusters should stabilize the monolayer of methane with the assistance of the carbon micropore walls. This structure model can explain the observed composition of methane and water molecules.

Acknowledgment. This work was partially funded by the Grant in-Aid for Scientific Research on Priority Areas No. 288 "Carbon Alloys" from the Japanese government.

References and Notes

(1) Sloan, E. D., Jr. *Clathrate Hydrate of Natural Gases*; Marcel Dekker: New York, 1990.
(2) Fleyfel, F.; Song, K. Y.; Kook, A.; Martin, R.; Kobayashi, R. *J. Phys. Chem.* **1993**, *97*, 6722.
(3) Sparks, K.; Texter, J. W. *J. Phys. Chem.* **1992**, *96*, 11022.
(4) Handa, Y. P.; Stupin, D. *J. Phys. Chem.* **1992**, *96*, 8599.
(5) Cha, S. B.; Ouar, H.; Wildeman, T. R.; Sloan, E. D. *J. Phys. Chem.* **1988**, *92*, 6492.
(6) Seator, N. A.; Walton, J. P. R. B.; Quirke, N. *Carbon* **1989**, *27*, 855.
(7) Cracknell, R. F.; Gubbins, K. E.; Madddox, M.; Nicholson, D. *Acc. Chem. Res.* **1995**, *28*, 281.
(8) Bojan, M. J.; Cheng, E.; Cole, M. W.; Steele, W. A. *Adsorption* **1996**, *2*, 51.
(9) Kaneko, K. *Colloid Surf.* **1996**, *109*, 309.
(10) Kaneko, K.; Fukuzaki, N.; Ozeki, S. *J. Chem. Phys.* **1987**, *87*, 776.
(11) Imai, J.; Souma, M.; Ozeki, S.; Suzuki, T.; Kaneko, K. *J. Phys. Chem.* **1991**, *95*, 9955.
(12) Iiyama, T.; Nishikawa, K.; Otowa, T.; Kaneko, K. *J. Phys. Chem.* **1995**, *99*, 10078.
(13) Iiyama, T.; Nishikawa, K.; Suzuki, T.; Kaneko, K. *Chem. Phys. Lett.* **1997**, *274*, 152.
(14) Fujie, K.; Minagawa, S.; Suzuki, T.; Kaneko, K. *Chem. Phys. Lett.* **1995**, *236*, 427.
(15) Müller, E. A.; Rull, L. F.; Vega, L. F. Gubbins, K. E. *J. Phys. Chem.* **1996**, *100*, 1189.
(16) Steele, W. A. *Surf. Sci.* **1973**, *36*, 317.
(17) Suzuki, T.; Kaneko, K.; Gubbins, K. E. *Langmuir* **1997,** *13*, 2545.
(18) Kaneko, K.; Ishii, C. *Colloid, Surf.* **1992**, *67*, 203.
(19) Setoyama, N.; Suzuki, T.; Kaneko, K. *Carbon*, in press.
(20) Hanzawa, Y.; Kaneko, K. *Langmuir* **1997**, *13*, 5803.
(21) Kaneko, K.; Hanzawa, Y.; Iiyama, T.; Kanda, T.; Suzuki, T. *Adsorption*, in press.
(22) Matranga, K. R.; Myers, A. L.; Galndt, E. D. *Chem. Eng. Sci.* **1992**, *47*, 1569.